We are IntechOpen, the world's leading publisher of Open Access books Built by scientists, for scientists

6,900
Open access books available

185,000
International authors and editors

200M
Downloads

Our authors are among the

154
Countries delivered to

TOP 1%
most cited scientists

12.2%
Contributors from top 500 universities



WEB OF SCIENCE™

Selection of our books indexed in the Book Citation Index in Web of Science™ Core Collection (BKCI)

Interested in publishing with us?
Contact book.department@intechopen.com

Numbers displayed above are based on latest data collected.
For more information visit www.intechopen.com



Chapter 1

Piezoelectric Actuators for Functionally Graded Plates-Nonlinear Vibration Analysis

Farzad Ebrahimi

Additional information is available at the end of the chapter

http://dx.doi.org/10.5772/52407

1. Introduction

Functionally graded materials (FGMs) are a new generation of composite materials wherein the material properties vary continuously to yield a predetermined composition profile. These materials have been introduced to benefit from the ideal performance of its constituents, e.g., high heat/corrosion resistance of ceramics on one side, and large mechanical strength and toughness of metals on the other side. FGMs have no interfaces and are hence advantageous over conventional laminated composites. FGMs also permit tailoring of material composition to optimize a desired characteristic such as minimizing the maximum deflection for a given load and boundary conditions, or maximizing the first frequency of free vibration, or minimizing the maximum principal tensile stress. As a result, FGMs have gained potential applications in a wide variety of engineering components or systems, including armor plating, heat engine components and human implants. FGMs are now developed for general use as structural components and especially to operate in environments with extremely high temperatures. Low thermal conductivity, low coefficient of thermal expansion and core ductility have enabled the FGM materials to withstand higher temperature gradients for a given heat flux. Structures made of FGMs are often susceptible to failure from large deflections, or excessive stresses that are induced by large temperature gradients and/or mechanical loads. It is therefore of prime importance to account for the geometrically nonlinear deformation as well as the thermal environment effect to ensure more accurate and reliable structural analysis and design.

The concept of developing smart structures has been extensively used for active control of flexible structures during the past decade [1-3]. In this regard, the use of axisymmetric piezoelectric actuators in the form of a disc or ring to produce motion in a circular or annular substrate plate is common in a wide range of applications including micro-pumps and mi-

INTECH
open science | open minds

© 2013 Ebrahimi; licensee InTech. This is an open access article distributed under the terms of the Creative Commons Attribution License (http://creativecommons.org/licenses/by/3.0), which permits unrestricted use, distribution, and reproduction in any medium, provided the original work is properly cited.

cro-valves [4, 5], devices for generating and detecting sound [6] and implantable medical devices [7]. They may also be useful in other applications such as microwave micro-switches where it is important to control distortion due to intrinsic stresses [8]. Also in recent years, with the increasing use of smart material in vibration control of plate structures, the mechanical response of FGM plates with surface-bonded piezoelectric layers has attracted some researchers' attention. Since this area is relatively new, published literature on the free and forced vibration of FGM plates is limited and most are focused on the cases of the linear problem. Among those, a 3-D solution for rectangular FG plates coupled with a piezoelectric actuator layer was proposed by Reddy and Cheng [9] using transfer matrix and asymptotic expansion techniques. Wang and Noda [10] analyzed a smart FG composite structure composed of a layer of metal, a layer of piezoelectric and an FG layer in between, while He et al. [11] developed a finite element model for studying the shape and vibration control of FG plates integrated with piezoelectric sensors and actuators. Yang et al. [12] investigated the nonlinear thermo-electro-mechanical bending response of FG rectangular plates that are covered with monolithic piezoelectric actuator layers on the top and bottom surfaces of the plate. More recently, Huang and Shen [13] investigated the dynamics of an FG plate coupled with two monolithic piezoelectric layers at its top and bottom surfaces undergoing nonlinear vibrations in thermal environments. In addition, finite element piezothermoelasticity analysis and the active control of FGM plates with integrated piezoelectric sensors and actuators was studied by Liew et al. [14] and the temperature response of FGMs using a nonlinear finite element method was studied by Zhai et al. [15]. All the aforementioned studies focused on the rectangular-shaped plate structures. To the authors' best knowledge, no researches dealing with the nonlinear vibration characteristics of the circular functionally graded plate integrated with the piezoelectric layers have been reported in the literature except the author's recent works in presenting an analytical solution for the free axisymmetric linear vibration of piezoelectric coupled circular and annular FGM plates [16-20] and investigating the applied control voltage effect on piezoelectrically actuated nonlinear FG circular plate [21] in which the thermal environment effects are not taken in to account.

Consequently, a non-linear dynamics and vibration analysis is conducted on pre-stressed piezo-actuated FG circular plates in thermal environment. Nonlinear governing equations of motion are derived based on Kirchhoff's-Love hypothesis with von-Karman type geometrical large nonlinear deformations. Dynamic equations and boundary conditions including thermal, elastic and piezoelectric couplings are formulated and solutions are derived. An exact series expansion method combined with perturbation approach is used to model the non-linear thermo-electro-mechanical vibration behavior of the structure. Numerical results for FG plates with various mixture of ceramic and metal are presented in dimensionless forms. A parametric study is also undertaken to highlight the effects of the thermal environment, applied actuator voltage and material composition of FG core plate on the nonlinear vibration characteristics of the composite structure. The new features of the effect of thermal environment and applied actuator voltage on free vibration of FG plates and some meaningful results in this chapter are helpful for the application and the design of nuclear reactors, space planes and chemical plants, in which functionally graded plates act as basic elements.

http://dx.doi.org/10.5772/52407

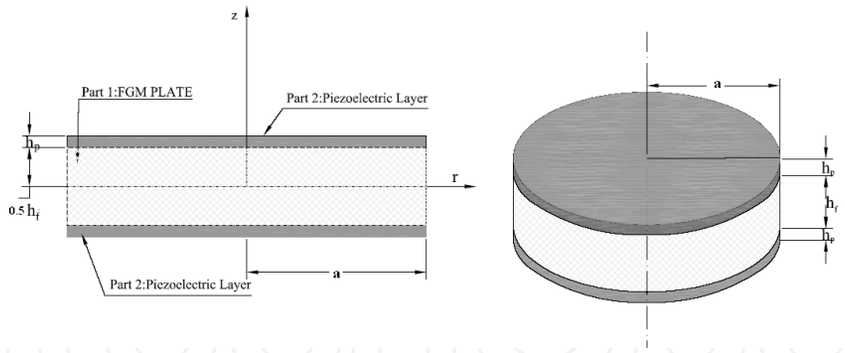


Figure 1. FG circular plate with two piezoelectric actuators.

2. Functionally graded materials (FGM)

Nowadays, not only can FGM easily be produced but one can control even the variation of the FG constituents in a specific way. For example in an FG material made of ceramic and metal mixture, we have:

$$V_m + V_c = 1 \tag{1}$$

in which V_c and V_m are the volume fraction of the ceramic and metallic part, respectively. Based on the power law distribution [22], the variation of V_c vs. thickness coordinate *(z)* with its origin placed at the middle of thickness, can be expressed as:

$$V_c = (z/h_f + 1/2)^n \quad , n \geq 0 \tag{2}$$

in which h_f is the FG core plate thickness and n is the FGM volume fraction index (see Figure 1). Note that the variation of both constituents (ceramics and metal) is linear when *n=1*. We assume that the inhomogeneous material properties, such as the modulus of elasticity *E*, densityρ, thermal expansion coefficient α and the thermal conductivity κ change within the thickness direction *z* based on Voigt's rule over the whole range of the volume fraction [23] while Poisson's ratio υ is assumed to be constant in the thickness direction [24] as:

$$\begin{aligned} E(z) &= (E_c - E_m)V_c(z) + E_m, \\ \rho(z) &= (\rho_c - \rho_m)V_c(z) + \rho_m \\ \alpha(z) &= (\alpha_c - \alpha_m)V_c(z) + \alpha_m, \\ \nu(z) &= \nu \\ \kappa(z) &= (\kappa_c - \kappa_m)V_c(z) + \kappa_m \end{aligned} \tag{3}$$

where subscripts m and c refer to the metal and ceramic constituents, respectively. After substituting Vc from Eq. (2) into Eqs. (3), material properties of the FGM plate are determined in the power law form-the same as those proposed by Reddy and Praveen [22]:

$$\begin{aligned} E_f(z) &= (E_c - E_m)(z/h_f + 1/2)^n + E_m, \\ \rho_f(z) &= (\rho_c - \rho_m)(z/h_f + 1/2)^n + \rho_m, \\ \kappa_f(z) &= (\kappa_c - \kappa_m)(z/h_f + 1/2)^n + \kappa_m, \\ \alpha_f(z) &= (\alpha_c - \alpha_m)(z/h_f + 1/2)^n + \alpha_m \end{aligned} \tag{4}$$

3. Thermal environment

Assume a piezo-laminated FGM plate is subjected to a thermal environment and the temperature variation occurs in the thickness direction and 1D temperature field is assumed to be constant in the *r-θ* plane of the plate. In such a case, the temperature distribution along the thickness can be obtained by solving a steady-state heat transfer equation

$$-\frac{d}{dz}\left[\kappa(z)\frac{dT}{dz}\right] = 0 \tag{5}$$

in which

$$\kappa(z) = \begin{cases} \kappa_p & \left(h_f/2 < z < h_p + h_f/2\right) \\ \kappa_f(z) & \left(-h_f/2 < z < h_f/2\right) \\ \kappa_p & \left(-h_p - h_f/2 < z < -h_f/2\right) \end{cases} \tag{6}$$

$$\kappa(z) = \begin{cases} \kappa_p & \left(h_f/2 < z < h_p + h_f/2\right) \\ \kappa_f(z) & \left(-h_f/2 < z < h_f/2\right) \\ \kappa_p & \left(-h_p - h_f/2 < z < -h_f/2\right) \end{cases} \tag{7}$$

where κ_p and κ_f are the thermal conductivity of piezoelectric layers and FG plate, respectively. Eq. (5) is solved by imposing the boundary conditions as

$$\begin{aligned} T_p\big|_{z=h_p+h_f/2} &= T_U \\ \tilde{T}_p\big|_{z=-h_p-h_f/2} &= T_L \end{aligned} \tag{8}$$

and the continuity conditions

$$\begin{aligned} T_p\big|_{z=h_f/2} &= T_f\big|_{z=h_f/2} = T_1, \\ T_f\big|_{z=-h_f/2} &= \tilde{T}_p\big|_{z=-h_f/2} = T_2, \\ \kappa_p \frac{dT_p(z)}{dz}\bigg|_{z=h_f/2} &= \kappa_c \frac{dT_f(z)}{dz}\bigg|_{z=h_f/2}, \\ \kappa_p \frac{d\tilde{T}_p(z)}{dz}\bigg|_{z=-h_f/2} &= \kappa_m \frac{dT_f(z)}{dz}\bigg|_{z=-h_f/2} \end{aligned} \tag{9}$$

The solution of Eq.(5) with the aforementioned conditions can be expressed as polynomial series:

$$T_p(z) = T_1 + \frac{T_U - T_1}{h_p}\left(z - h_f/2\right) \tag{10}$$

$$\tilde{T}_p(z) = T_L + \frac{T_2 - T_L}{h_p}\left(z + h_f/2 + h_p\right) \tag{11}$$

and

$$\begin{aligned} T_f(z) = A_0 + A_1\left(\frac{z}{h_f}+\frac{1}{2}\right) + A_2\left(\frac{z}{h_f}+\frac{1}{2}\right)^{n+1} + A_3\left(\frac{z}{h_f}+\frac{1}{2}\right)^{2n+1} + A_4\left(\frac{z}{h_f}+\frac{1}{2}\right)^{3n+1} + \\ A_5\left(\frac{z}{h_f}+\frac{1}{2}\right)^{4n+1} + A_6\left(\frac{z}{h_f}+\frac{1}{2}\right)^{5n+1} + O(z)^{6n+1} \end{aligned} \tag{12}$$

where constants T_1, T_2 and A_j can be found in Appendix A.

4. Nonlinear piezo-thermo-electric coupled FG circular plate system

It is assumed that an FGM circular plate is sandwiched between two thin piezoelectric layers which are sensitive in both circumferential and radial directions as shown in Figure 1 and the structure is in thermal environment; also, the piezoelectric layers are much thinner than the FGM plate, i.e., $h_p << h_f$.An initial large deformation exceeding the linear range is imposed on the circular plate and a von-Karman type nonlinear deformation is adopted in the analysis. The von-Karman type nonlinearity assumes that the transverse nonlinear deflection w is much more prominent than the other two inplane deflections.

4.1. Nonlinear strain-displacement relations

Based on the Kirchhoff-Love assumptions, the strain components at distance z from the middle plane are given by

$$\begin{aligned} \varepsilon_{rr} &= \bar{\varepsilon}_{rr} + zk_{rr}, \\ \varepsilon_{\theta\theta} &= \bar{\varepsilon}_{\theta\theta} + zk_{\theta\theta}, \\ \varepsilon_{r\theta} &= \bar{\varepsilon}_{r\theta} + zk_{r\theta} \end{aligned} \tag{13}$$

where the z-axis is assumed positive outward. Here$\bar{\varepsilon}_{rr}$,$\bar{\varepsilon}_{\theta\theta}$, $\bar{\varepsilon}_{r\theta}$are the engineering strain components in the median surface, andk_{rr},$k_{\theta\theta}$, $k_{r\theta}$are the curvatures which can be expressed in terms of the displacement components. The relations between the middle plane strains and the displacement components according to the von-Karman type nonlinear deformation and Sander's assumptions [25] are defined as:

$$\begin{aligned} \bar{\varepsilon}_{rr} &= \frac{\partial u_r}{\partial r} + \frac{1}{2}\left(\frac{\partial w}{\partial r}\right)^2, \\ \bar{\varepsilon}_{\theta\theta} &= \frac{1}{r}\frac{\partial u_\theta}{\partial \theta} + \frac{u_r}{r} + \frac{1}{2}\left(\frac{1}{r}\frac{\partial w}{\partial \theta}\right)^2, \\ \bar{\varepsilon}_{r\theta} &= \frac{1}{r}\frac{\partial u_r}{\partial \theta} + \frac{\partial u_\theta}{\partial r} - \frac{u_\theta}{r} + \left(\frac{1}{r}\frac{\partial w}{\partial r}\right)\frac{\partial w}{\partial \theta} \end{aligned} \tag{14}$$

$$\begin{aligned} \kappa_{rr} &= -\frac{\partial^2 w}{\partial r^2}, \\ \kappa_{\theta\theta} &= -\frac{1}{r}\frac{\partial w}{\partial r} - \frac{1}{r^2}\frac{\partial^2 w}{\partial \theta^2}, \\ \kappa_{r\theta} &= -\frac{1}{r}\left(\frac{\partial^2 w}{\partial r \partial \theta}\right) + \frac{1}{2r^2}\frac{\partial w}{\partial \theta} \end{aligned} \tag{15}$$

http://dx.doi.org/10.5772/52407

whereu_r,u_θ ,w represent the corresponding components of the displacement of a point on the middle plate surface. Substituting Eqs. (14) and (15) into Eqs. (13), the following expressions for the strain components are obtained

$$\begin{aligned}
\varepsilon_{rr} &= \frac{\partial u_r}{\partial r} + \frac{1}{2}\left(\frac{\partial w}{\partial r}\right)^2 - z\frac{\partial^2 w}{\partial r^2}, \\
\varepsilon_{\theta\theta} &= \frac{1}{r}\frac{\partial u_\theta}{\partial \theta} + \frac{u_r}{r} + \frac{1}{2}\left(\frac{1}{r}\frac{\partial w}{\partial \theta}\right)^2 - z\left(\frac{1}{r}\frac{\partial w}{\partial r} + \frac{1}{r^2}\frac{\partial^2 w}{\partial \theta^2}\right), \\
\varepsilon_{r\theta} &= \frac{1}{r}\frac{\partial u_r}{\partial \theta} + \frac{\partial u_\theta}{\partial r} - \frac{u_\theta}{r} + \left(\frac{1}{r}\frac{\partial w}{\partial r}\right)\frac{\partial w}{\partial \theta} + 2z\left(-\frac{1}{r}\left(\frac{\partial^2 w}{\partial r \partial \theta}\right) + \frac{1}{2r^2}\frac{\partial w}{\partial \theta}\right)
\end{aligned} \tag{16}$$

For a circular plate with axisymmetric oscillations, the strain expressions are simplified to

$$\begin{aligned}
\varepsilon_{rr} &= \frac{\partial u_r}{\partial r} + \frac{1}{2}\left(\frac{\partial w}{\partial r}\right)^2 - z\frac{\partial^2 w}{\partial r^2}, \\
\varepsilon_{\theta\theta} &= \frac{u_r}{r} - \frac{z}{r}\frac{\partial w}{\partial r}, \\
\varepsilon_z &= \gamma_{r\theta} = \gamma_{\theta z} = \gamma_{zr} = 0
\end{aligned} \tag{17}$$

4.2. Force and moment resultants

The stress components in the FG core plate in terms of strains based on the generalized Hooke's Law using the plate theory approximation of $\sigma_z \approx 0$in the constitutive equations are defined as [26];

$$\sigma_r^f = \frac{E(z)}{1-\nu^2}(\varepsilon_r + \nu\varepsilon_\theta) - \frac{E(z)\alpha(z)}{1-\nu}\Delta T \tag{18}$$

$$\sigma_\theta^f = \frac{E(z)}{1-\nu^2}(\varepsilon_\theta + \nu\varepsilon_r) - \frac{E(z)\alpha(z)}{1-\nu}\Delta T \tag{19}$$

where E(z), ν(z) and α(z) are Young's modulus, Poisson's ratio and coefficient of thermal expansion of the FGM material, respectively, as expressed in Eq.(4), where $\Delta T = T(z) - T_0$ is temperature rise from the stress-free reference temperature (T_0) which is assumed to exist at a temperature of T_0=0 and $T(z)$ is presented in Eqs. (10)-(12).

The moments and membrane forces include both mechanical and electric components as

$$\begin{aligned} N_r &= N_r^m - N_r^e - N_r^t, \\ N_\theta &= N_\theta^m - N_\theta^e - N_\theta^t, \\ M_r &= M_r^m - M_r^e - M_r^t, \\ M_\theta &= M_\theta^m - M_\theta^e - M_\theta^t \end{aligned} \tag{20}$$

where the superscripts m, e, and t, respectively, denote the mechanical, electric, and temperature components. Mechanical forces and moments of the thin circular plate made of functionally graded material can be expressed as

$$(N_r^m, N_\theta^m) = \int_{-h_f/2}^{h_f/2} (\sigma_{rr}, \sigma_{\theta\theta}) dz \tag{21}$$

$$(M_r^m, M_\theta^m) = \int_{-h_f/2}^{h_f/2} (\sigma_{rr}, \sigma_{\theta\theta}) z dz \tag{22}$$

$$(N_{r\theta}^m, M_{r\theta}^m) = \int_{-h_f/2}^{h_f/2} (1, z) \sigma_{r\theta} dz \tag{23}$$

Substituting Eqs. (13) and (18),(19) into Eqs. (22)-(23) gives the following constitutive relations for mechanical forces and moments of FG plate :

$$\begin{aligned} N_r^m &= D_1(\bar{\varepsilon}_{rr} + \nu \bar{\varepsilon}_{\theta\theta}), \\ N_\theta^m &= D_1(\bar{\varepsilon}_{\theta\theta} + \nu \bar{\varepsilon}_{rr}) \end{aligned} \tag{24}$$

$$\begin{aligned} M_r^m &= D_2(\kappa_{rr} + \nu \kappa_{\theta\theta}), \\ M_\theta^m &= D_2(\kappa_{\theta\theta} + \nu \kappa_{rr}) \end{aligned} \tag{25}$$

$$N_r^t = N_\theta^t = \int_{-h_t/2}^{h_t/2} \frac{\alpha(z) E(z)}{1-\nu} \Delta T(z)\, dz \tag{26}$$

$$M_r^t = M_\theta^t = \int_{-h_t/2}^{h_t/2} \frac{\alpha(z) E(z)}{1-\nu} \Delta T(z)\, z dz \tag{27}$$

in which the coefficients of D_1 and D_2 in the above equations are related to the plate stiffness and are given by

$$D_1 = \int_{-h_f/2}^{h_f/2} \frac{E_f(z)}{1-\nu_f^2} dz,$$
$$D_2 = \int_{-h_f/2}^{h_f/2} z^2 \frac{E_f(z)}{1-\nu_f^2} dz \tag{28}$$

It is assumed that the piezoelectric layers are sensitive in both radial and circumferential directions and the piezoelectric permeability constants e_{31}=e_{32}. Hence, the electric membrane forces and bending moments are induced by the converse piezoelectric effect on the piezoelectric actuators, and these forces vary linearly across the plate thickness as [27];

$$N_r^e = N_\theta^e = -e_{31}\left(V_z^t + V_z^b\right)/2, \tag{29}$$

$$M_r^e = M_\theta^e = -e_{31}\left(h_f + h_p\right)\left(V_z^t - V_z^b\right)/2, \tag{30}$$

in which V_z^t and V_z^b are the control voltages applied to the top and bottom piezoelectric layers, respectively.

4.3. System electromechanical equations

Axisymmetric free oscillation equations of the piezoelectric coupled circular FG plate in thermal environment can be derived from the generic piezoelectric shell equations using four system parameters: two Lame parameters, A_1=1, A_2=r, where r is the radial distance measured from the center, and two radii, R_1=∞, R_2=∞ [28,29] as

$$\frac{\partial(rN_r)}{\partial r} - N_\theta = 0 \tag{31}$$

$$\frac{1}{r}\frac{\partial(rQ_{rz})}{\partial r} + N_r\frac{\partial^2 w}{\partial r^2} + N_{\theta\theta}\left(\frac{1}{r}\frac{\partial w}{\partial \theta}\right) - I_1\frac{\partial^2 w}{\partial t^2} = 0 \tag{32}$$

in which I_1=$\left(\int_{-h_f/2}^{h_f/2}\rho_f(z)dz\right)$and the transverse shear component Q_{rz} is related to moments as

$$Q_{rz} = \frac{1}{r}\left[\frac{\partial(rM_r)}{\partial r} - M_\theta\right] \tag{33}$$

Note that only the normal radial strain keeps the quadratic nonlinear term. Substituting all force/moment components and strain-displacement equations into the radial and transverse equations (31), (32) yields

$$r\frac{\partial}{\partial r}\left[\frac{1}{r}\frac{\partial}{\partial r}\left(r^2 N_r^m\right)\right] = -\frac{Y}{2}\left(\frac{\partial w}{\partial r}\right)^2 + \frac{\partial}{\partial r}\left[r^2\frac{\partial}{\partial r}\left(N_r^e + N_r^t\right)\right] + \nu\, r\frac{\partial}{\partial r}\left(N_r^e + N_r^t\right) \tag{34}$$

$$\begin{aligned}&\frac{D_2}{r}\frac{\partial}{\partial r}\left(r\frac{\partial}{\partial r}\left[\frac{1}{r}\frac{\partial}{\partial r}\left(r\frac{\partial}{\partial r}w(r,\,t)\right)\right]\right) = \\ &-I_1\frac{\partial^2 w}{\partial t^2} + \frac{1}{r}\frac{\partial}{\partial r}\left[r\frac{\partial w}{\partial r}\left(N_r^m - N_r^e - N_r^t\right)\right] - \frac{1}{r}\frac{\partial}{\partial r}\left[r\frac{\partial}{\partial r}\left(M_r^e + M_r^t\right)\right]\end{aligned} \tag{35}$$

in which $Y = \left(\int_{-h_f/2}^{h_f/2} E_f(z)dz\right)$ and boundary conditions at the center of the plate with axisymmetric oscillations are defined as

$$(1)\ \text{Plate center}\ (r=0): Slope: \frac{\partial w}{\partial r} = 0 \tag{36a}$$

$$Radial\ force: N_{rr}^m: finite \tag{36b}$$

Boundary conditions for the simply supported (immovable) circumference are defined as:

Plate circumference (r=a):

$$w = 0 \tag{37a}$$

$$\frac{\partial}{\partial r}(rN_r^m) - \nu N_r^m = r\frac{\partial}{\partial r}(N_r^e + N_r^t) \tag{37b}$$

$$-D_2\left(\frac{\partial^2 w}{\partial r^2} + \frac{\nu}{r}\frac{\partial w}{\partial r}\right) = (M_r^e + M_r^t) \tag{37c}$$

It is further assumed that the control potentials on the top and bottom piezoelectric actuators are of equal magnitudes and opposite signs, i.e., $V_z^t = -V_z^b = \hat{V}$ and the plate is subjected

http://dx.doi.org/10.5772/52407

to a uniform temperature excitation of *T(z)*. Accordingly, the electric and temperature induced forces and moments can be defined as:

$$N_r^e = N_\theta^e = 0 \tag{38a}$$

$$M_r^e = M_\theta^e = M^e = -e_{31}\left(h_f + h_p\right)\hat{V}, \tag{38b}$$

$$N_\theta^t = N_r^t = N^t, \tag{39a}$$

$$M_\theta^t = M_r^t = M^t, \tag{39b}$$

Using these force and moment expressions, one can further simplify the open-loop plate equations and boundary conditions:

$$r\frac{\partial}{\partial r}\left[\frac{1}{r}\frac{\partial}{\partial r}\left(r^2 N_r^m\right)\right] = -\frac{Y}{2}\left(\frac{\partial w}{\partial r}\right)^2 \tag{40}$$

$$\frac{D_2}{r}\frac{\partial}{\partial r}\left(r\frac{\partial}{\partial r}\left[\frac{1}{r}\frac{\partial}{\partial r}\left(r\frac{\partial}{\partial r}w(r,t)\right)\right]\right) = -I_1\frac{\partial^2 w}{\partial t^2} + \frac{1}{r}\frac{\partial}{\partial r}\left[r\frac{\partial w}{\partial r}\left(N_r^m - N^t\right)\right] \tag{41}$$

Boundary conditions become

Plate center (r=0):

$$Slope: \left.\frac{\partial w}{\partial r}\right|_{r=0} = 0 \tag{42a}$$

$$Radial\ force: \left.N_r^m\right|_{r=0}: finite \tag{42b}$$

Plate circumference (r=a):

$$\left.w\right|_{r=a} = 0 \tag{43a}$$

$$\left[\frac{\partial}{\partial r}(rN_r^m) - \nu N_r^m\right]_{r=a} = 0 \tag{43b}$$

$$\left[-D_2\left(\frac{\partial^2 w}{\partial r^2}+\frac{\nu}{r}\frac{\partial w}{\partial r}\right)\right]_{r=a}=(M^e+M^t) \tag{43c}$$

4.4. Simplification and Normalization

Solutions of the transverse displacement w and radial force N_r^m of the above open-loop plate equations and boundary conditions can be expressed as a summation of a static component and a dynamic component as

$$w(r,t)=w_s(r)+w_d(r,t) \tag{44a}$$

$$N_r^m(r,t)=N_{r_s}^m(r,t)+N_{r_d}^m(r,t) \tag{44b}$$

where $w_s(r)$and $N_{r_s}^m(r,\ t)$ are the static solutions, $w_d(r,\ t)$and $N_{r_d}^m(r,\ t)$ are the dynamic solutions, and the subscripts s and d, respectively, denote the static and dynamic solutions. Accordingly, the solution procedure can be divided into two parts. The first part deals with the nonlinear static solutions, and the second part deals with the dynamic solutions. In addition, normalized dimensionless quantities are adopted in the static and dynamic analyses. These dimensionless quantities are defined by known geometrical and material parameters [30]:

- radial distance: $y=(r/a)^2$,
- transverse deflection: $\overline{w}_s=\sqrt{3(1-\nu^2)}\dfrac{w_s}{h_f}$,
- slope: $X_s(y)=y\dfrac{d\overline{w}_s}{dy}$
- static force: $Y_s^m(y)=\left(a^2N_{r_s}^m/4D_2\right)y$
- radial distance: $x=(r/a)$,
- dynamic deflection: $\overline{w}_d=\sqrt{3(1-\nu^2)}\dfrac{w_d}{h_f}$,
- dynamic force: $Y_d^m(y)=\left(a^2N_{r_d}^m/D_2\right)$
- voltage: $V=[3(1-\nu^2)]^{1/2}e_{31}(h_f+h_p)\hat{V}/\left(2D_2h_f\right)$
- temperature load: $T^*=\left(a^2N^t/4D_2\right)$

Substituting these normalized dimensionless quantities into the open-loop plate equations and boundary conditions of axisymmetric plate oscillations and separating the static parts from the dynamic parts gives the static equations and dynamic equations with their associated boundary conditions:

(1) Static Equations *and Boundary Conditions*

$$y^2 \frac{d^2 X_s}{dy^2} = X_s Y_s^m - T * yX_s \tag{45}$$

$$y^2 \frac{d^2 Y_s^m}{dy^2} = -\frac{1}{2}\left(X_s\right)^2, \qquad 0 < y < 1 \tag{46}$$

Boundary conditions at center y = 0:

$$X_s\big|_{y=0} = 0 \tag{47a}$$

$$Y_s^m\big|_{y=0} = 0 \tag{47b}$$

Boundary conditions on circumference y = 1:

$$\left[\left(1+\nu\right)Y_s^m - 2\frac{dY_s^m}{dy}\right]_{y=1} = 0 \tag{48a}$$

$$\left[\left(1-\nu\right)\frac{X_s}{y} - 2\frac{dX_s^m}{dy}\right]_{y=1} = V\big|_{y=1} \tag{48b}$$

(2) Dynamic Equations and Boundary Conditions

$$x\frac{\partial}{\partial x}\left(\frac{1}{x}\frac{\partial}{\partial x}\left[x^2 Y_d^m\right]\right) = -2\left[\frac{d\overline{w}_s}{dx}\frac{\partial \overline{w}_d}{\partial x} - \frac{1}{2}\left(\frac{\partial \overline{w}_d}{\partial x}\right)^2\right] \tag{49}$$

$$\frac{1}{x}\frac{\partial}{\partial x}\left\{x\frac{\partial}{\partial x}\left[\frac{1}{x}\frac{\partial}{\partial x}\left(x\frac{\partial}{\partial x}(\overline{w}_d)\right)\right]\right\}=$$
$$-\frac{I_1 a^4}{D_2}\frac{\partial^2\overline{w}_d}{\partial t^2}+\frac{1}{x}\frac{\partial}{\partial x}\left[xY_d^m\frac{d\overline{w}_s}{dx}+\frac{4}{x}Y_s^m\frac{\partial\overline{w}_d}{\partial x}+xY_d^m\frac{\partial\overline{w}_d}{\partial x}\right]-4\hat{T}\frac{1}{x}\frac{\partial}{\partial x}\left(x\frac{\partial\overline{w}_d}{\partial x}\right) \quad (50)$$
$$0<x<1$$

Boundary conditions at center $x = 0$:

$$\left.\frac{\partial\overline{w}_d}{\partial x}\right|_{x=0}=0 \quad (51a)$$

$$\left.Y_d^m\right|_{x=0}=finite \quad (51b)$$

Boundary conditions on circumference $x = 1$:

$$\left.\overline{w}_d\right|_{x=1}=0 \quad (52a)$$

$$\left[\nu\frac{\partial}{\partial x}(Y_d^m)+(1-\nu)Y_d^m\right]_{x=1}=0 \quad (52b)$$

$$\left[\frac{\partial^2\overline{w}_d}{\partial x^2}+\nu\frac{\partial\overline{w}_d}{\partial x}\right]_{x=1}=0 \quad (52c)$$

5. Static Solutions

For the nonlinear static equations and boundary conditions of the boundary value problem derived above, static solutions of slopes $X_s(y)$and forces $Y_s^m(y)$can be represented in (exact) series expansion forms [30]:

$$X_s(y)=\sum_{i=1}^{\infty}A_i y^i \quad (53a)$$

$$Y_s^m(y) = \sum_{i=1}^{\infty} B_i y^i \qquad 0 \le y \le 1 \tag{53b}$$

where A_i and B_i are constant coefficients. Substituting the series solutions, Eqs. (53a&*b)*, into static equations, Eqs. (45) & (46), and grouping coefficients of y^i one can obtain the recurrence equations for coefficients A_i and B_i:

$$A_i = \frac{1}{i(i-1)} \sum_{j=1}^{i-1} A_j B_{i-j} - \hat{T} A_{i-1} \tag{54a}$$

$$B_i = \frac{-1}{2i(i-1)} \sum_{j=1}^{i-1} A_j A_{i-j}, \qquad i = 2,3,4,... \tag{54b}$$

It is observed that only A_1 and B_1 are independent constants, and the others are dependent. As long as A_1 and B_1 are determined by the boundary conditions, other coefficients A_i and B_i can be calculated from the recurrence equations. Accordingly, static series solutions are completed. The series solutions of $Y_s^m(y)$and $X_s(y)$satisfy the boundary conditions at y = 0, Eqs. (47a,b). Substituting the assumed series solutions$Y_s^m(y)$and $X_s(y)$ into the boundary conditions at y = 1, Eqs. (48a,b), yields

$$\sum_{i=1}^{\infty} \left[(1+\nu-2i) B_i \right] = 0 \tag{55a}$$

$$\sum_{i=1}^{\infty} \left[(1-\nu-2i) A_i \right] = V \tag{55b}$$

A_i and B_i can be determined from the nonlinear algebraic equations Eqs. (55a,b) using the Newton-Raphson iteration method [31]. Define

$$\alpha(A_1, B_1) = \sum_{i=1}^{\infty} \left[(1-\nu-2i) A_i \right] - V \tag{56a}$$

$$\beta(A_1, B_1) = \sum_{i=1}^{\infty} \left[(1+\nu-2i) B_i \right] \tag{56b}$$

$$\bar{A}_1 = A_1 + \Delta_1 \tag{57a}$$

$$\bar{B}_1 = B_1 + \Delta_2 \tag{57b}$$

in which

$$\Delta_1 = \frac{1}{\Delta}\left[\beta\left(A_1, B_1\right)\frac{\partial}{\partial B_1}\alpha\left(A_1, B_1\right) - \alpha\left(A_1, B_1\right)\frac{\partial}{\partial B_1}\beta\left(A_1, B_1\right)\right] \tag{58a}$$

$$\Delta_2 = \frac{1}{\Delta}\left[\alpha\left(A_1, B_1\right)\frac{\partial}{\partial A_1}\beta\left(A_1, B_1\right) - \beta\left(A_1, B_1\right)\frac{\partial}{\partial A_1}\alpha\left(A_1, B_1\right)\right] \tag{58b}$$

and

$$\Delta = \det\begin{bmatrix} \frac{\partial}{\partial A_1}\alpha\left(A_1, B_1\right) & \frac{\partial}{\partial B_1}\alpha\left(A_1, B_1\right) \\ \frac{\partial}{\partial A_1}\beta\left(A_1, B_1\right) & \frac{\partial}{\partial B_1}\beta\left(A_1, B_1\right) \end{bmatrix} \neq 0 \tag{58c}$$

$\bar{A}_1$and $\bar{B}_1$are, respectively, the iteration values of A_1 and B_1 ; $\Delta_1$and Δ_2 are the correction factors of A_1 and B_1 at each iteration. The partial derivatives$\partial\alpha/\partial A_1$,$\partial\alpha/\partial B_1$,$\partial\beta/\partial A_1$ and $\partial\beta/\partial B_1$, can be determined from the definitions of $\alpha(A_1, B_1)$and$\beta(A_1, B_1)$. These iterations are repeated until they reach their prescribed limits, say $|\alpha|$, $|\beta|$, $|\Delta_1|$ and $|\Delta_2|$ are smaller than 10^{-4}. Accordingly, a set of A_1 and B_1 are determined for a set of given control voltages V and temperatures$T$. Using the recurrence equations, one can determine all other A_i's and B_i's, and further the nonlinear static solutions of slope $X_s(y)$ and static force$Y_s^m(y)$. Knowing the slope, one can determine the static deflections $\bar{w}_s$and w_s of the nonlinear circular plate subject to voltage and temperature excitations.

6. Dynamic Solutions

It is assumed that the FG circular plate is oscillating in the vicinity of the nonlinearly deformed static equilibrium position. FG index, voltage and temperature effects to the natural frequencies and amplitude/frequency relations are investigated in this section. First, linearized eigenvalue equations are solved using the exact series solutions. Then nonlinear ampli-

http://dx.doi.org/10.5772/52407

tude and frequency relations of nonlinear large amplitude free vibrations are investigated using the Galerkin method and the perturbation method.

6.1. Eigenvalue Equations

Neglect the nonlinear terms in the normalized dynamic equations, and then assume following harmonic solutions of displacement and dynamic force

$$\bar{w}_d(x,t) = R_d(x)\sin(\omega_n t) \tag{59a}$$

$$Y_d^m(x,t) = S_d(x)\sin(\omega_n t) \tag{59b}$$

where ω_n is the natural frequency; $R_d(x)$and $S_d(x)$are the (linear) eigenfunctions or mode shape functions of $\bar{w}_d(x,\ t)$and$Y_d^m(x,\ t)$, respectively. $R_d(x)$defines the mode shape function, and $S_d(x)$ defines the spatial force distribution. Both $R_d(x)$and $S_d(x)$ have to satisfy the boundary conditions, and they are also assumed in the series expansion forms. Substituting Eqs. (59a, b) into the dynamic equations and boundary conditions, Eqs. (49)-(52), yields

$$x\frac{d}{dx}\left(\frac{1}{x}\frac{d}{dx}\left[x^2 S_d(x)\right]\right) = -2\frac{d\bar{w}_s}{dx}\frac{dR_d}{dx} \tag{60}$$

$$\begin{aligned}&\frac{1}{x}\frac{d}{dx}\left\{x\frac{d}{dx}\left[\frac{1}{x}\frac{d}{dx}\left(x\frac{d}{dx}(R_d(x))\right)\right]\right\} = \\ &\lambda R_d(x) + \frac{1}{x}\frac{d}{dx}\left[2xS_d(x)\frac{d\bar{w}_s}{dx} + \frac{4}{x}Y_s^m\frac{dR_d}{dx}\right] - 4\hat{T}\frac{1}{x}\frac{d}{dx}\left[x\frac{dR_d}{dx}\right],\ 0<x<1\end{aligned} \tag{61}$$

where λ is the eigenvalue and$\lambda = I_1\frac{a^4}{D_2}\omega_n^2$. Boundary conditions become

1. Center x=0:

$$\left.\frac{dR_d}{dx}\right|_{x=0} = 0 \tag{62a}$$

$$S_d(x)\big|_{x=0} : finite \tag{62b}$$

2. Circumference x=1:

$$R_d\big|_{x=1} = 0 \tag{63a}$$

$$\left[\nu \frac{d}{dx}\left[S_d(x)\right] + (1-\nu) S_d(x)\right]_{x=1} = 0 \tag{63b}$$

$$\left[\frac{d^2 R_d}{dx^2} + \nu \frac{dR_d}{dx}\right]_{x=1} = 0 \tag{63c}$$

Again, assume the eigenfunctions take the series expansion forms:

$$R_d(x) = \sum_{i=0}^{\infty} a_i x^{2i} \tag{64a}$$

$$S_d(x) = \sum_{i=0}^{\infty} b_i x^{2i} \tag{64b}$$

where a_i andb_i, are constants determined by eigenvalue equations and boundary conditions. The series solutions $R_d(x)$ and$S_d(x)$satisfy the boundary conditions at x = 0, Eqs. (62a,b). Assume a_i andb_i, be represented by the linear combinations of independent constantsa_0, $a_1$and b_0.

$$a_i = f_{i1} a_0 + f_{i2} a_1 + f_{i3} b_0 \tag{65a}$$

$$b_i = g_{i1} a_0 + g_{i2} a_1 + g_{i3} b_0 \ , \quad i = 1, 2, 3, \ldots \tag{65b}$$

where f_{ij} and $g_{ij}$are to be determined. Substituting the series expressions of modes $R_d(x)$and forces $S_d(x)$ into the dynamic equations, one can derive a set of recurrence equations of a_i andb_i. Then, using expressions of a_i and b_i of Eqs. (65a, b), one can further determine the coefficients f_{ij} and g_{ij} f_{01}=1, f_{02}=f_{03}=0; f_{11}=0, f_{12}=1, f_{13}=0; $g_{ik} = -\frac{2}{i(i+1)} \sum_{j=1}^{i} j f_{jk} A_{i-j+1}$, i=1, 2, 3, ... , k=1, 2, 3.,g_{01}=0, g_{02}=0, g_{03}=1; $f_{21} = \lambda / 64$, $f_{23} = A_1 / 8$, $f_{33} = \left[A_1 g_{13} + 4 f_{23}(B_1 - T^*) + A_2\right] / 36$, $f_{32} = \left\{\lambda + 32 B_2 + 16\left[A_1 g_{12} + 4 f_{22}(B_1 - T^*)\right]\right\} / 24$, $f_{31} = \left[A_1 g_{11} + 4 f_{21}(B_1 - T^*)\right] / 36$, $f_{22} = (B_1 - T^*) / 4$

http://dx.doi.org/10.5772/52407

$$f_{(i+2)k}=\left[\lambda f_{ik}-16T^{*}(i+1)^{2}+8(i+1)\times\sum_{j=1}^{i+1}\left(2jf_{ik}B_{i-k+2}+A_{j}g_{(i-j+1)k}\right)\right]\left[4(i+1)(i+2)\right]^{-2}\ i=2,\ 3,\ 4,\ \ldots,$$

and $k=1,\ 2,\ 3$.

Substituting these coefficients into the boundary conditions at x = 1, one can obtain an explicit matrix representation of the eigenvalue equation.

$$\begin{bmatrix} h_{11} & h_{12} & h_{13} \\ h_{21} & h_{22} & h_{23} \\ h_{31} & h_{32} & h_{33} \end{bmatrix}\begin{bmatrix} a_0 \\ a_1 \\ b_0 \end{bmatrix}=\begin{bmatrix}0\end{bmatrix} \tag{66}$$

where h_{ij} are defined by

$$h_{1k}=\sum_{i=0i1}^{\infty}f_{ik} \tag{67a}$$

$$h_{2k}=\sum_{i=0}^{\infty}\left[i\nu+i\left(2i-1\right)\right]f_{ik}\quad,\quad k=1,2,3. \tag{67b}$$

$$h_{3k}=\sum_{i=0}^{\infty}\left[2i\nu+\left(1-\nu\right)\right]g_{ik}\quad,\quad k=1,2,3. \tag{67c}$$

These h_{ik} coefficients are functions of eigenvalues λ, and accordingly, the determinant of the coefficient matrix leads to a nonlinear characteristic equation. Using the Newton-Raphson iteration method [31], one can calculate eigenvalues and furthermore natural frequencies and mode shape functions of the nonlinear FG circular plate.

6.2. Nonlinear Large Amplitude Free Vibrations

In this section, the perturbation method is used to investigate the nonlinear large amplitude effect to natural frequencies of the piezoelectric laminated FG circular plate. Assume an approximate solution of the nonlinear response $\overline{w}_{d}(x,\ t)$ be a product of a spatial function $\overline{w}_{d}^{*}(x)$ and a temporal function $f(t)$;

$$\overline{w}_{d}(x,t)=\overline{w}_{d}^{*}(x)f(t) \tag{68}$$

where $\overline{w}_d^*(x)$ is a test function satisfying the boundary conditions:

1. Plate center x=0: $\left.\frac{\partial \overline{w}_d^*}{\partial x}\right|_{x=0}=0$

2. Plate circumference x=1: $\overline{w}_d^*|_{x=1}=0$,

$$\left[\frac{\partial^2 \overline{w}_d^*}{\partial x^2}+\nu\frac{\partial \overline{w}_d^*}{\partial x}\right]_{x=1}=0 \tag{69}$$

Substituting Eq. (68) into the dynamic equation Eq. (49) and using the Galerkin method, one can derive a nonlinear equation for $f(\tau)$

$$f_{,\tau\tau}+f(\tau)+\mu_1 f^2(\tau)+\mu_2 f^3(\tau)=0 \tag{70}$$

where $\tau=\omega t$ and μ_1 and μ_2 are the nonlinear coefficient functions, ω is defined by

$$\omega^2=\left(c_1+c_3\right)/c_2\,. \tag{71}$$

c_1,c_2 and $c_3$are defined by integrals:

$$c_1=\int_0^1\left\{\overline{w}_d^*(x)\frac{d}{dx}\left\{x\frac{d}{dx}\left[\frac{1}{x}\frac{d}{dx}\left(x\frac{d}{dx}(\overline{w}_d^*(x))\right)\right]\right\}\right\}dx \tag{72a}$$

$$c_2=\int_0^2\left(\overline{w}_d^*(x)\right)^2 x dx \tag{72b}$$

$$c_3=-\int_0^1\overline{w}_d^*(x)\frac{d}{dx}\left[\frac{4}{x}Y_s^m\frac{d\overline{w}_d^*}{dx}+2xN_{r_d}^{*l}\frac{d\overline{w}_s}{dx}-4T*x\frac{d\overline{w}_d^*}{dx}\right]dx \tag{72c}$$

in which $N_{r_d}^{*l}(x)$and $N_{r_d}^{*n}(x)$ are the linear and nonlinear force components. The nonlinear coefficient functions μ_1 and $\mu_1$are defined by

$$\mu_1=c_4/\left(c_1+c_3\right) \tag{73a}$$

http://dx.doi.org/10.5772/52407

$$\mu_2 = c_5 / \left(c_1 + c_3 \right) \tag{73b}$$

where c_4 and $c_5$are defined by integrals:

$$c_4 = -\int_0^1 \overline{w}_d^*(x) \frac{d}{dx}\left[2xN_{r_d}^{*n}(x) \frac{d\overline{w}_s(x)}{dx} + N_{r_d}^{*l}(x) \frac{d\overline{w}_d^*(x)}{dx} \right] dx \tag{74a}$$

$$c_5 = -\int_0^1 \overline{w}_d^*(x) \frac{d}{dx}\left[xN_{r_d}^{*n}(x) \frac{d\overline{w}_d^*(x)}{dx} \right] dx \tag{74b}$$

The linear and nonlinear force components are written as

$$N_{r_d}^{*l}(x) = \frac{1}{x^2} \int_0^1 G(x,\xi) \frac{1}{\xi} \frac{d\overline{w}_s}{d\xi} \frac{d\overline{w}_d^*}{d\xi} d\xi \tag{75a}$$

$$\overline{N}_{r_d}^{*n}(x) = \frac{1}{4x^2} \int_0^1 G(x,\xi) \frac{1}{\xi} \left(\frac{d\overline{w}_d^*}{d\xi} \right)^2 d\xi \tag{75b}$$

The kernel function

$$G(x,\xi) = \begin{cases} \left[1 - \left((1+\nu)/(1-\nu) \right) \xi^2 \right] x^2 & x < \xi, \\ \left[1 - \left((1+\nu)/(1-\nu) \right) x^2 \right] \xi^2 & x \geq \xi, \end{cases} \tag{76}$$

Since the mode shape functions of the linear free vibrations were determined previously, it is convenient to select the mode shape functions as the trial functions,

$$\overline{w}_d^*(x) = R_d(x), \tag{77a}$$

$$N_{r_d}^{*l}(x) = S_d(x), \quad 0 \leq x \leq 1; \tag{77b}$$

and the frequency can be selected as the natural frequencies determined previously. Using the Krylov-Bogoliubov-Mitropolsky perturbation method [32] and solving the nonlinear dynamic equation Eq. (70), one can obtain the amplitude-frequency relation as

$$p = \frac{\omega}{\omega_n} = 1 + \frac{1}{24}\left(9\mu_2 - 10\mu_1^2\right)\hat{a}^2 + \frac{5}{8}\mu_1\mu_2\hat{a}^3 + \ldots \tag{78}$$

where $\omega$is the (nonlinear vibration) frequency; $\omega_n$is the natural frequency; $\hat{a}$is the dimensionless vibration amplitude; and μ_1 and μ_2 are the nonlinear coefficient functions. Note that the ratio is unity, i.e.,$p=\omega/\omega_n=1$, if the system is linear. Once the coefficients μ_1 and $\mu_2$are calculated, one can further evaluate the amplitude and frequency relations of the nonlinear circular plate subjected to temperature excitations and control voltages.

7. Results and Discussions

Temperature effects of nonlinear static deformations, control voltages, and linear and nonlinear free vibrations of a simply supported piezoelectric laminated functionally graded circular plate are investigated in this section.

7.1. Comparison studies

To ensure the accuracy of the present analysis, an illustrative example is solved. The relevant material properties are listed in Table 1. Since there are no appropriate comparison results available for the problems being analyzed in this chapter, we decided to verify the validity of the obtained results by comparing with those of the FEM results. Our FEM model for piezo-FG plate consists of a 3D 8-noded solid element with number of total nodes 26950, number of total elements 24276, 4 DOF per node (3 translation, temperature) in the host plate element and 6 DOF per node (3 translation, temperature, voltage and magnetic properties) in the piezoelectric element. The finite element model has been programmed by the authors, while the standard bilinear interpolations have been employed in finite element approximations.

Table 2 compares the present results of normalized dimensionless central deflections $W_s=\sqrt{3(1-\nu^2)}(w_s/h_f)$ with finite element solutions in analyzing the effect of normalized dimensionless piezoelectric voltages $V=[3(1-\nu^2)]^{1/2}e_{31}(h_f+h_p)V^*/(2D_2h_f)$ to the normalized dimensionless center deflections at various normalized temperatures ($T^*=\left(a^2N^t/4D_2\right)$) in which a nonlinear deflection-voltage relationship can be observed. As seen from Table 2 the maximum estimated difference of the proposed solution with finite element method is about 0.079%, and a close correlation between these results validates the proposed method of solution.

In general, a higher temperature induces higher deflections of the plate, and the deflection at each temperature is attenuated when the control voltage increases and the effect of imposed

http://dx.doi.org/10.5772/52407

voltage on the center deflection is nonlinear and this effect is predominant in lesser voltage amounts. This effect can also be seen in the case of considering the temperature environment effect. For example, when $T^* = 0.2$by increasing the imposed voltage from 0.6 to 1.2 (100%) the normalized dimensionless center deflections increases about 46.8%, while it increases about 34.5% when the imposed voltage increases from 1.2 to 2.4 (100%). In the case of $T^* = 0.5$by increasing the imposed voltage from 0.6 to 1.2 (100%) the normalized dimensionless center deflection increases about 36.5% while it increases about 28.7% when the imposed voltage increases from 1.2 to 2.4 (100%).

Material	**Property**					
	E (GPa)	ρ (kg/m^3)	ν	α $(1/°C)$	κ (W/mK)	d_{31}, d_{32} (m/V)
Aluminum	70	2707	0.3	23e-6	204	-
Alumina	380	3800	0.3	7.4e-6	10.4	-
PZT	63	7600	0.3	1.2e-4	0.17	1.79e-10

Table 1. Material properties [13].

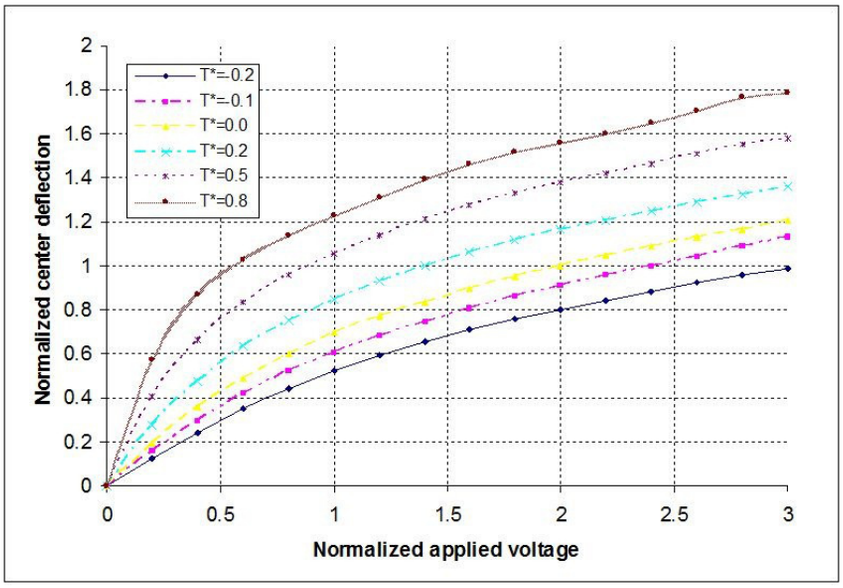


Figure 2. Effect of applied voltage to the normalized center deflection for various normalized temperatures $T^* = \left(a^2 N^t / 4D_2\right)$ (Metal plate)

Normalized Voltage (V)	Normalized Temperature(T^*)					
	$T^*=0$			$T^*=0.2$		
	Present	FEM	Diff. (%)	Present	FEM	Diff. (%)
0	0	0	0	0	0	0
0.4	0.3537	0.3538	0.041	0.8659	0.8663	0.044
0.8	0.5982	0.5985	0.048	1.1347	1.1352	0.046
1.2	0.7681	0.7685	0.055	1.3118	1.3126	0.060
1.6	0.8925	0.8930	0.057	1.4601	1.4610	0.062
2	0.9924	0.9930	0.065	1.5581	1.5592	0.070
2.4	1.0777	1.0784	0.068	1.6458	1.6470	0.074
2.8	1.1509	1.1517	0.071	1.7653	1.7666	0.076
	$T^*=0.5$			$T^*=0.8$		
	Present	FEM	Diff. (%)	Present	FEM	Diff. (%)
0	0	0	0	0	0	0
0.4	0.6633	0.6636	0.043	0.8659	0.8663	0.044
0.8	0.9569	0.9573	0.045	1.1347	1.1352	0.046
1.2	1.1380	1.1387	0.058	1.3118	1.3126	0.060
1.6	1.2746	1.2754	0.060	1.4601	1.4610	0.062
2.0	1.3776	1.3785	0.068	1.5581	1.5592	0.070
2.4	1.4643	1.4653	0.072	1.6458	1.6470	0.074
2.8	1.5510	1.5522	0.075	1.7653	1.7666	0.076

Table 2. Values of the normalized dimensionless center deflections with respect to the normalized dimensionless piezoelectric voltages for various normalized temperatures computed by two methods (present series solution and FEM) (v=0.3, n=1000)

7.2. Parametric studies

Having validated the foregoing formulations, we began to study the large amplitude vibration behavior of FG laminated circular plate subjected to thermo-electro-mechanical loading. The results for laminated plates with isotropic substrate layers (that is, the substrate is purely metallic or purely ceramic) and with graded substrate layers (various n) are given in both tabular and graphical forms.

To investigate the effect of the applied actuator voltage on the non-linear thermo-electromechanical vibration, the nonlinear normalized center deflection of various graded plates under various applied normalized voltages is tabulated in Table 3.

http://dx.doi.org/10.5772/52407

Normalized Temp. (T^*)	FGM index (n) / Normalized Voltage (V)							
	Metal				n=10			
	V=0.2	V=0.3	V=0.5	V=1	V=0.2	V=0.3	V=0.5	V=1
0.0	0.1820	0.2724	0.3924	0.6925	0.1206	0.1805	0.2601	0.4590
0.2	0.2738	0.3869	0.5213	0.8573	0.1815	0.2564	0.3455	0.5681
0.4	0.3654	0.5010	0.6421	0.9949	0.2422	0.3320	0.4255	0.6593
0.6	0.4706	0.6169	0.7596	1.1164	0.3119	0.4089	0.5034	0.7399
0.8	0.6071	0.7400	0.8808	1.2329	0.4024	0.4905	0.5838	0.8171
(T^*)					n=0.5			
	V=0.2	V=0.3	V=0.5	V=1	V=0.2	V=0.3	V=0.5	V=1
0.0	0.0992	0.1484	0.2138	0.3773	0.0939	0.1405	0.2024	0.3572
0.2	0.1492	0.2108	0.2840	0.4670	0.1413	0.1996	0.2689	0.4422
0.4	0.1991	0.2729	0.3498	0.5420	0.1885	0.2584	0.3312	0.5132
0.6	0.2564	0.3361	0.4138	0.6082	0.2428	0.3183	0.3919	0.5759
0.8	0.3308	0.4032	0.4799	0.6716	0.3132	0.3818	0.4544	0.6360
(T^*)					Ceramic (n=0)			
	V=0.2	V=0.3	V=0.5	V=1	V=0.2	V=0.3	V=0.5	V=1
0.0	0.0838	0.1255	0.1807	0.3190	0.0716	0.1072	0.1544	0.2725
0.2	0.1261	0.1782	0.2401	0.3948	0.1078	0.1522	0.2051	0.3373
0.4	0.1683	0.2307	0.2957	0.4582	0.1438	0.1971	0.2527	0.3915
0.6	0.2168	0.2841	0.3499	0.5142	0.1852	0.2428	0.2989	0.4393
0.8	0.2796	0.3409	0.4057	0.5678	0.2389	0.2912	0.3466	0.4851

Table 3. FGM index and normalized voltage effects to the nonlinear center deflection

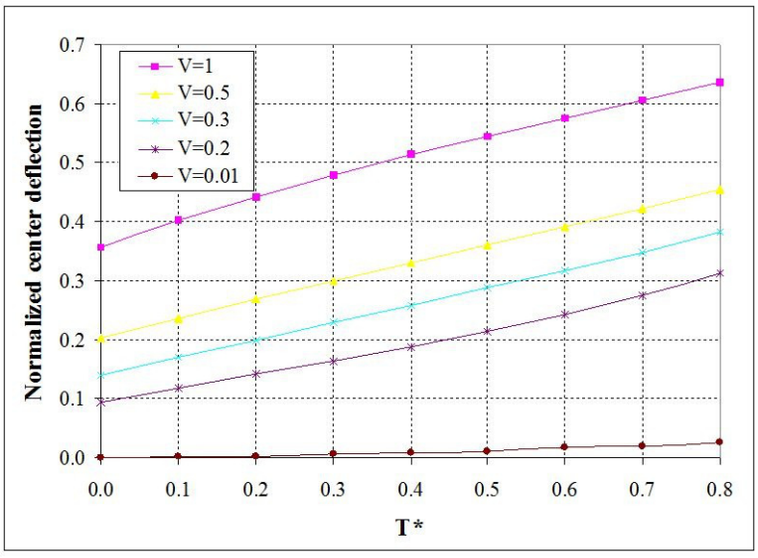


Figure 3. Normalized Temperature effects to the center deflection for various values of Voltages (n=0.5)

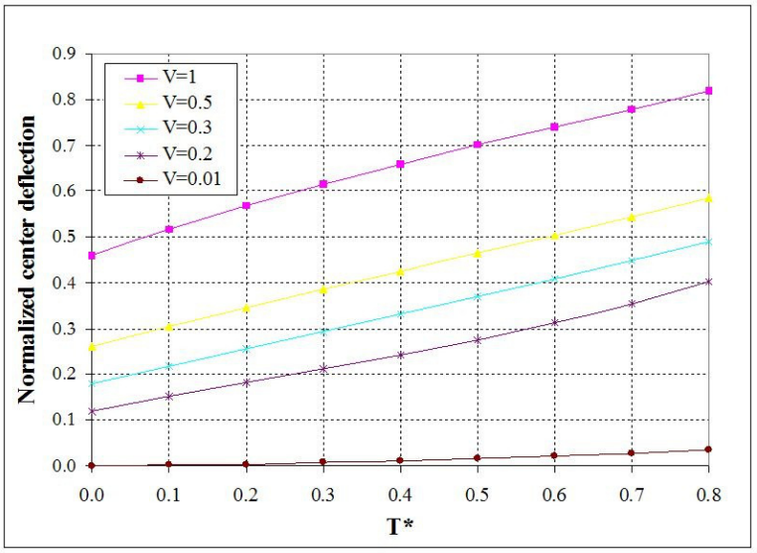


Figure 4. Normalized Temperature effects to the center deflection for various values of Voltages (n=10)

For instance, Figs. 3 and 4. depict the normalized temperature and voltage effects on the center deflection of two graded plates (n=0.5 n=10). It shows that increasing the normalized temperature makes the center deflection increase in various voltages, but this effect is predominant at higher voltages. Figures 5~6 depict the effect of FGM index on the non-linear thermo-electro-mechanical behavior (center deflection) of FGM plates with different normalized applied voltages in logarithmic scale. It is also obvious from these figures that, by increasing the material gradients, the normalized center deflection would be increased in various temperature fields, and it is also demonstrated that larger thermal gradients will lead to greater deflections. This trend can be seen in various material gradients, which means that the non-linear deflection can be controlled by applying the appropriate voltage in the piezoelectric actuator layers.

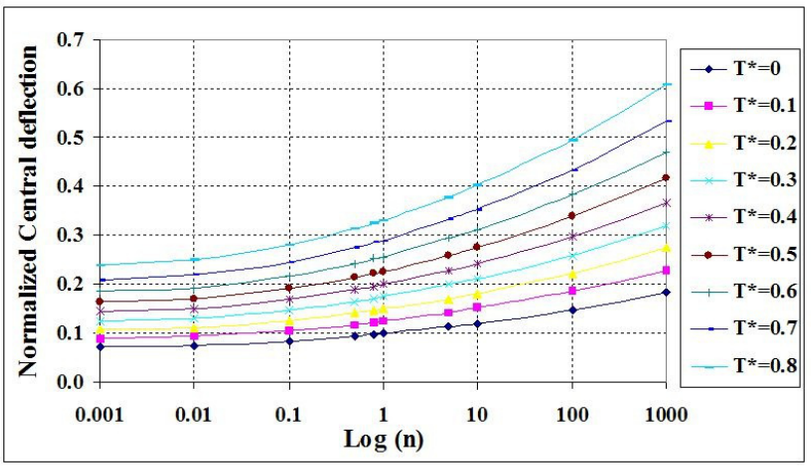


Figure 5. FGM index effects on nonlinear center deflection for various normalized temperature (V=0.2)

http://dx.doi.org/10.5772/52407

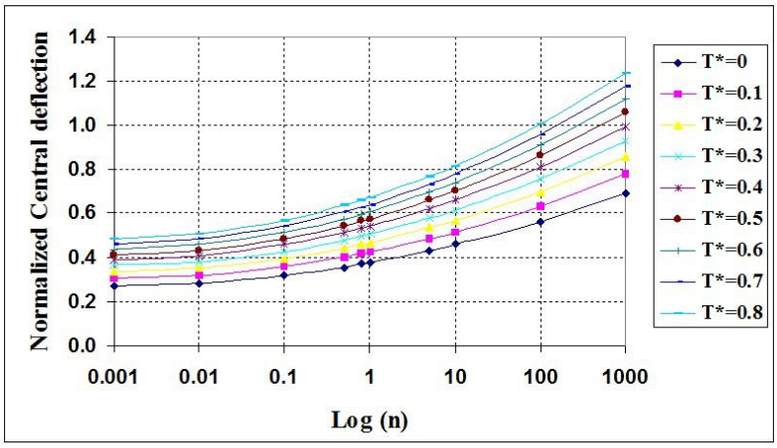


Figure 6. FGM index effects on nonlinear center deflection for various normalized temperature (V=1)

Normalized Voltage (V)	FGM index (n) / Normalized Temp. (T*)							
	Metal				n=10			
	Normalized Temperature (T*)				Normalized Temperature(T*)			
	0	0.2	0.5	0.8	0	0.2	0.5	0.8
0.0	*4.8891*	*4.4249*	*3.5293*	*2.3669*	*5.5359*	*5.0103*	*3.9962*	*2.6800*
0.4	*5.5796*	*5.67452*	*5.92735*	*6.49712*	*6.3178*	*6.4253*	*6.7116*	*7.3567*
0.8	*6.7141*	*7.26308*	*8.00595*	*8.71889*	*7.6024*	*8.2240*	*9.0652*	*9.8724*
1.2	*7.7799*	*8.452*	*9.37002*	*10.1564*	*8.8092*	*9.5702*	*10.6097*	*11.5001*
1.6	*8.6394*	*9.33903*	*10.3511*	*11.2809*	*9.7824*	*10.5746*	*11.7206*	*12.7734*
2.0	*9.3329*	*10.1399*	*11.2449*	*12.2285*	*10.5677*	*11.4814*	*12.7326*	*13.8464*
2.4	*9.9414*	*10.8734*	*12.0351*	*13.0241*	*11.2567*	*12.3120*	*13.6274*	*14.7472*
2.8	*10.5104*	*11.4499*	*12.6036*	*13.7116*	*11.9010*	*12.9647*	*14.2711*	*15.5257*
	0	0.2	0.5	0.8	0	0.2	0.5	0.8
0.0	*7.4121*	*6.7083*	*5.3506*	*3.5883*	*11.2882*	*10.2165*	*8.1487*	*5.4648*
0.4	*8.4589*	*8.6028*	*8.9861*	*9.8499*	*12.8825*	*13.1017*	*13.6854*	*15.0009*
0.8	*10.1789*	*11.0111*	*12.1374*	*13.2182*	*15.5020*	*16.7694*	*18.4846*	*20.1307*
1.2	*11.7947*	*12.8136*	*14.2054*	*15.3975*	*17.9627*	*19.5145*	*21.6340*	*23.4497*
1.6	*13.0977*	*14.1584*	*15.6927*	*17.1023*	*19.9472*	*21.5625*	*23.8992*	*26.0460*
2.0	*14.1491*	*15.3725*	*17.0478*	*18.5389*	*21.5483*	*23.4116*	*25.9629*	*28.2339*
2.4	*15.0716*	*16.4845*	*18.2458*	*19.7451*	*22.9533*	*25.1051*	*27.7874*	*30.0708*
2.8	*15.9342*	*17.3585*	*19.1076*	*20.7874*	*24.2670*	*26.4362*	*29.0999*	*31.6582*

Table 4. FGM index and normalized temperature effects to the first natural frequency for various normalized voltages.

We examine in this section the effect of control voltages and thermal environment on the vibration characteristics of the piezoelectric laminated circular FG plate for various FGM in-

dexes. To this end, Table 4 as well as the Figures 4.1~4.3 show the nonlinear relationships between the first natural frequencies$\omega_i a^2\sqrt{I_1/D_2}$, versus the normalized temperature in various normalized control voltages$V$. These free vibrations are assumed to be in the vicinity of the nonlinearly deformed static equilibrium position.

Also, the effect of normalized temperature on the first natural frequency of the FG circular plate for various FGM indexes under various normalized control voltage is investigated and tabulated in Table 4, while the voltage-dependent first natural frequency changes are plotted in Figures 7~9 for various temperatures. It is seen that the imposed voltage has a significant effect on the first natural frequency of the structure, and by increasing the imposed voltage, the first natural frequency increases in a nonlinear manner. For instance, for the FGM plate with n=10 by increasing the imposed voltage from 0 to 0.2 the first natural frequency increases about 4.84%, while by increasing the voltage from 0.2 to 0.3 the first natural frequency increases about 15.12%.

It is seen that the imposed thermal environment has a significant effect on the first natural frequency of the structure, and by increasing the imposed temperature, the first natural frequency decreases in a nonlinear manner. However, this thermal tendency of decreasing the natural frequency can be compensated and corrected with the control voltages V, as shown in Fig. 7. ~ 8.

Frequency variations of large amplitude oscillations with temperature and applied voltage changes are also investigated and plotted in Figure 6. There are two sets of curves in this figure. The first set has no control voltages, and the second set has control voltages. It is observed that the control voltages actually reduce the nonlinear frequency and amplitude ratios, i.e.,$P \to 1$. Accordingly, the nonlinear frequency and amplitude ratios can be actively controlled and the nonlinear effects reduced, i.e., the ratio is approaching to 1- the linear case. Other studies of the second natural frequency also suggest that the second natural frequency exhibits very much similar phenomena of the first natural frequency.

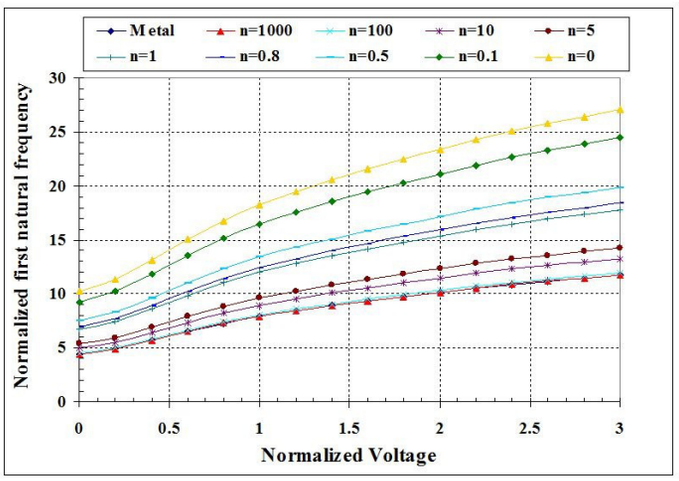


Figure 7. Effect of normalized voltage to first natural frequency for various FGM indexes (T*=0.2)

http://dx.doi.org/10.5772/52407

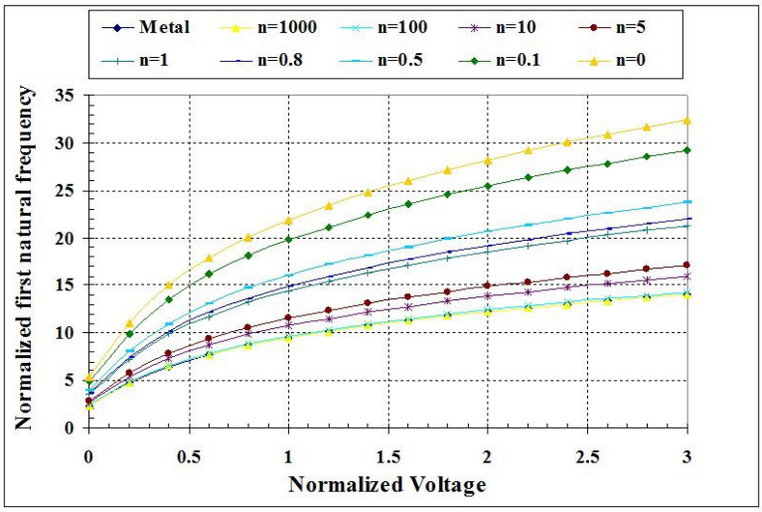


Figure 8. Effect of normalized voltage to first natural frequency for various FGM indexes (T*=0.8)

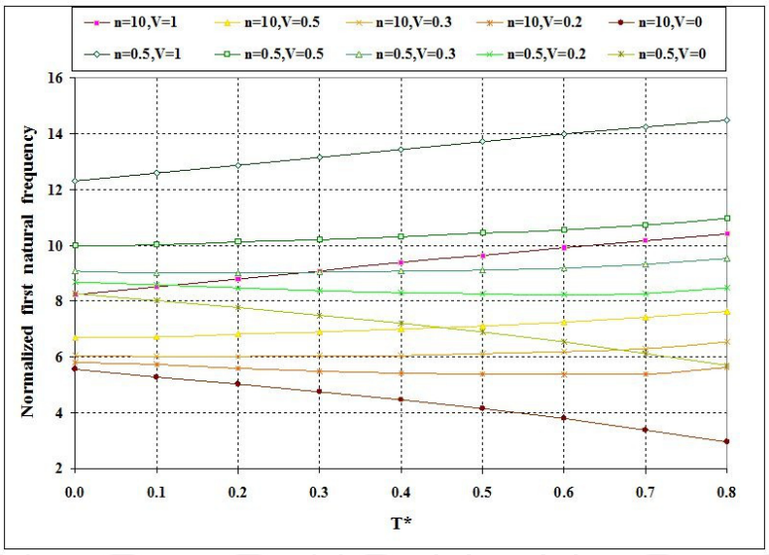


Figure 9. Effects of normalized temperature on the normalized first natural frequency for various normalized voltages (n=10,n=0.5)

8. Summary and Conclusions

A piezoelectric bounded circular FG plate subjected to temperature changes and control voltages is investigated based on classical plate theory, including the effects of the thermal gradient, piezothermoelasticity and von Karman type geometric nonlinearity. Nonlinear coupled open-loop plate equations in radial and transverse oscillations were derived first, and then the equations were simplified to an axisymmetric oscillation case. An exact solution technique based on series-type solutions is used to obtain piezothermoelastic solutions

for nonlinear static deformations and natural frequencies of the FG circular plate subjected to temperature and voltage excitations. Voltage controlled natural frequencies of the first mode at various temperatures are studied. It is observed that a higher temperature induces higher deflections of the plate, and the deflection at each temperature is attenuated when the control voltage increases, but this effect is predominant in higher voltages. Also by increasing the FGM gradient index the normalized center deflection will increase in a nonlinear manner in various temperature fields. It is seen that the imposed thermal environment has a significant effect on the natural frequency of the structure, and by increasing the imposed temperature, the natural frequency decreases in a nonlinear manner for various FGM indexes; this effect is predominant at higher temperatures. Both the nonlinear static deflections and natural frequencies are influenced by the temperatures and control voltages geometric and the static control voltages can be used to compensate nonlinear deflections.

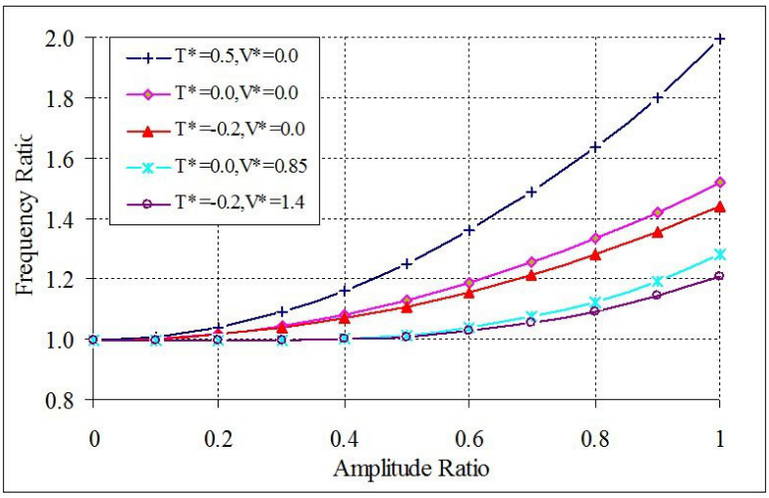


Figure 10. Temperature/control effects on amplitude dependent first natural frequency (for metal plate) – amplitude ratio: w/h_f, frequency ratio: (ω/ω_1)

Appendix A:

$$T_1 = T_2 + (T_U - T_L) - \frac{\kappa_c d + \kappa_m}{\kappa_m}(T_2 - T_L), \quad T_2 = T_L + \left[\frac{\kappa_m}{ch_f}(T_U - T_L)\right] \Big/ \left[\frac{\kappa_p}{h_p} + \frac{\kappa_c d + \kappa_m}{ch_f}\right]$$

$$A_0 = T_2, \qquad A_1 = \frac{T_1 - T_2}{c} \qquad A_2 = -\frac{T_1 - T_2}{c}\frac{\kappa_{cm}}{(N+1)\kappa_m}$$

$$A_3 = \frac{T_1 - T_2}{c}\frac{\kappa_{cm}^2}{(2N+1)\kappa_m^2} \qquad A_4 = -\frac{T_1 - T_2}{c}\frac{\kappa_{cm}^3}{(3N+1)\kappa_m^3}$$

$$A_5 = \frac{T_1 - T_2}{c}\frac{\kappa_{cm}^4}{(4N+1)\kappa_m^4} \qquad A_6 = -\frac{T_1 - T_2}{c}\frac{\kappa_{cm}^5}{(5N+1)\kappa_m^5}$$

http://dx.doi.org/10.5772/52407

where

$$\kappa_{cm} = \kappa_c - \kappa_m$$

$$c = 1 - \frac{1}{N+1}\frac{\kappa_{cm}}{\kappa_m} + \frac{1}{2N+1}\left(\frac{\kappa_{cm}}{\kappa_m}\right)^2 - \frac{1}{3N+1}\left(\frac{\kappa_{cm}}{\kappa_m}\right)^3 + \frac{1}{4N+1}\left(\frac{\kappa_{cm}}{\kappa_m}\right)^4 - \frac{1}{5N+1}\left(\frac{\kappa_{cm}}{\kappa_m}\right)^5$$

$$d = 1 - \frac{\kappa_{cm}}{\kappa_m} + \left(\frac{\kappa_{cm}}{\kappa_m}\right)^2 - \left(\frac{\kappa_{cm}}{\kappa_m}\right)^3 + \left(\frac{\kappa_{cm}}{\kappa_m}\right)^4 - \left(\frac{\kappa_{cm}}{\kappa_m}\right)^5$$

Acknowledgements

The work described in this chapter was funded by a grant from International University of Imam Khomeini (Grant No. 385022-1391) The author is grateful for this financial support.

Author details

Farzad Ebrahimi*

Address all correspondence to: f.ebrahimi@ikiu.ac.ir

Department of Mechanical Engineering, Faculty of Engineering, Imam Khomeini International University, Qazvin, Iran

References

[1] Peng, F., Ng, A., & Hu, Y. R. (2005). Actuator placement optimization and adaptive vibration control of plate smart structures. J. Intell. Mater. Syst. Struct. , 16-263.

[2] Dong, S., & Tong, L. (2001). Vibration control of plates using discretely distributed piezoelectric quasi-modal actuators/sensors. *AIAA J.*, 39-1766.

[3] Ray, M. C. (2003). Optimal control of laminated shells with piezoelectric sensor and actuator layers,. *AIAA J.*, 41-1151.

[4] Spencer, W. J., Corbett, W. T., Dominguez, L. R., & Shafer, B. D. (1978). An electronically controlled piezoelectric insulin pump and valves. *IEEE Trans. Sonics Ultrason.*, 25-153.

[5] Dong, S., Du, X., Bouchilloux, P., & Uchino, K. (2002). Piezoelectric ring-morph actuation for valve application. *J. Electroceram*, 8-155.

[6] Chee, C. Y. K., Tong, L., & Steve, G. P. (1998). A review on the modeling of piezoelectric sensors and actuators incorporated in intelligent structures,. *J. Intell. Mater. Syst. Struct.*, 9-3.

[7] Cao, L., Mantell, S., & Polla, D. (2001). Design and simulation of an implantable medical drug delivery system using microelectromechanical systems technology. *Sensors Actuators A*, 94-117.

[8] Chen, X., Fox, C. H. J., & Mc William, S. (2004). Optimization of a cantilever microswitch with piezoelectric actuation. *J. Intell. Mater. Syst. Struct.*, 15-823.

[9] Reddy, J. N., & Cheng, Z. Q. (2001). Three-dimensional solutions of smart functionally graded plates. *ASME J. Appl. Mech.*, 68-234.

[10] Wang, B. L., & Noda, N. (2001). Design of smart functionally graded thermo-piezoelectric composite structure. *Smart Mater. Struct.*, 10-189.

[11] He, X. Q., Ng, T. Y., Sivashanker, S., & Liew, K. M. (2001). Active control of FGM plates with integrated piezoelectric sensors and actuators. , Int. J. Solids Struct. , 38-1641.

[12] Yang, J., Kitipornchai, S., & Liew, K. M. (2004). Nonlinear analysis of thermo-electromechanical behavior of shear deformable FGM plates with piezoelectric actuators. *Int. J. Numer. Methods Eng.*, 59-1605.

[13] Huang, X. L., & Shen, H. S. (2006). Vibration and dynamic response of functionally graded plates with piezoelectric actuators in thermal environments. *J. Sound Vib.*, 289-25.

[14] Liew, K. M., He, X. Q., Ng, T. Y., & Kitipornchai, S. (2003). Finite element piezothermoelasticity analysis and the active control of FGM plates with integrated piezoelectric sensors and actuators. *Computational Mechanics*, 31-350.

[15] Zhai, P. C., Zhang, Q. J., & Yuan, R. Z. (1997). Influence of temperature dependent properties on temperature response and optimum design of C/M FGMs under thermal cyclic loading. *J. Wuhan Univ. Technol.*, 12-19.

[16] Ebrahimi, F., & Rastgoo, A. (2008). Free vibration analysis of smart annular FGM plates integrated with piezoelectric layers. *Smart Mater. Struct,*, 17(015044).

[17] Ebrahimi, F., & A.and, Rastgoo. (2008). An analytical study on the free vibration of smart circular thin FGM plate based on classical plate theory. *Thin-Walled Structures*, 46-1402.

[18] Ebrahimi, F., & Rastgoo, A. (2008). Free Vibration Analysis of Smart FGM Plates. *International Journal of Mechanical Systems Science and Engineering*, 2(2), 94-99.

[19] Ebrahimi, F., Rastgoo, A., & Kargarnovin, M. H. (2008). Analytical investigation on axisymmetric free vibrations of moderately thick circular functionally graded plate integrated with piezoelectric layers. *Journal of Mechanical Science and Technology*, 22(6), 1056-1072.

[20] Ebrahimi, F., Rastgoo, A., & Atai, A. A. (2009). Theoretical analysis of smart moderately thick shear deformable annular functionally graded plate. *European Journal of Mechanics- A/Solids*, 28-962.

[21] Ebrahimi, F., & Rastgoo, A. (2009). Nonlinear vibration of smart circular functionally graded plates coupled with piezoelectric layers. *Int J Mech Mater Des*, 5-157.

[22] Reddy, J. N., & Praveen, G. N. (1998). Nonlinear transient thermoelastic analysis of functionally graded ceramic-metal plate,. *Int. J. Solids Struct.*, 35-4457.

[23] Wetherhold, R. C., Seelman, S., & Wang, S. (1996). The use of functionally graded materials to eliminate or control thermal deformation. *Compos. Sci. Technol.*, 56-1099.

[24] Tanigawa, Y., Morishita, H., & Ogaki, S. (1999). Derivation of system of fundamental equations for a three dimensional thermoelastic field with nonhomogeneous material properties and its application to a semi infinite body. *J. Therm. Stresses*, 22-689.

[25] Brush, D. O., & Almroth, B. O. (1975). Buckling of Bars Plates and Shells,. *McGraw-Hill, New York*.

[26] Reddy, J. N. (1999). Theory and Analysis of Elastic Plates. *Taylor and Francis, Philadelphia*.

[27] Song, G., Sethi, V., & Lic, H. N. (2006). Vibration control of civil structures using piezoceramic smart materials: A review. *Engineering Structures*, 28-1513.

[28] Efraim, E., & Eisenberger, M. (2007). Exact vibration analysis of variable thickness thick annular isotropic and FGM plate,. *J. Sound Vib.*, 299-720.

[29] Tzou, H. S. (1993). Piezoelectric Shells-(Distributed Sensing and Control of Continua,. *Kluwer Dordrecht*.

[30] Zheng, X. J., & Zhou, Y. H. (1990). Analytical formulas of solutions of geometrically nonlinear equations of axisymmetric plates and shallow shells. *Acta Mech. Sinica*, 6(1), 69-81.

[31] William, H. P., Brain, P. F., & Sau, A. T. (1986). Numerical Recipes-the Art of Scientific Computing,. *Cambridge University Press, New York*.

[32] Nayfe, H., & Mook, D. T. (1979). Nonlinear Oscillations. *John Wiley, New York*.

IntechOpen

IntechOpen